CONDENSED MATTER PHYSICS

Gate tuning from exciton superfluid to quantum anomalous Hall in van der Waals heterobilayer

Qizhong Zhu, Matisse Wei-Yuan Tu, Qingjun Tong, Wang Yao*

Van der Waals heterostructures of two-dimensional (2D) materials provide a powerful approach toward engineering various quantum phases of matter. Examples include topological matter such as quantum spin Hall (QSH) insulator and correlated matter such as exciton superfluid. It can be of great interest to realize these vastly different quantum phases matter on a common platform; however, their distinct origins tend to restrict them to material systems of incompatible characters. Here, we show that heterobilayers of 2D valley semiconductors can be tuned through interlayer bias between an exciton superfluid, a quantum anomalous Hall insulator, and a QSH insulator. The tunability between these distinct phases results from the competition of Coulomb interaction with the interlayer quantum tunneling that has a chiral form in valley semiconductors. Our findings point to exciting opportunities for harnessing both protected topological edge channels and bulk superfluidity in an electrically configurable platform.

INTRODUCTION

In an exciton Bose-Einstein condensate, an electron and a hole pair into an exciton that can flow without dissipation. Confining electron and hole into two separate layers allows the exciton superfluid (ES) to manifest as counterflowing electrical supercurrents in the electron and hole layers (*1*, *2*). Van der Waals (vdW) heterostructures are ideal realizations of the double-layer geometry for exploring this correlated phase of matter driven by Coulomb interaction (*3*–*5*). Evidence of the counterflow supercurrents in the quantum Hall regime were recently reported in graphene double bilayers (*3*, *4*). High-temperature ES phases in the absence of magnetic field are also predicted in graphene (*6*) and transition metal dichalcogenide (TMD) double-layer heterostructures (*7*, *8*).

Quantum spin Hall (QSH) insulators are topological state of matter driven by the spin-orbit coupling, a single-particle relativistic effect (*9*, *10*). In two-dimensional (2D) crystals and their vdW heterostructures, the miniaturization in thickness can lead to a remarkable gate-tunable QSH phase, featuring helical edge states that can be electrically switched on/off inside the bulk gap (*11*–*14*). Electron flow in the helical QSH edge channel is protected from backscattering, except by the spin-flip scatters. Coupling the QSH insulator to the local magnetic moment in ferromagnetism can suppress the topological order in one spin species (*15*, *16*), turning QSH into the quantum anomalous Hall (QAH) insulator. QAH features a chiral edge state that is completely lossless with the absence of backward channel. The edge conducting channels of these topological phases of matter, as well as the bulk supercurrents in the ES, can have profound consequences in quantum electronics (*1*–*4*, *17*, *18*).

Here, we show the possibility of realizing these vastly different quantum phases of matter with gate switchability on a single platform of a TMD heterobilayer. What makes this system unique is the coexistence of strong Coulomb interaction that favors spontaneous s-wave interlayer electron-hole coherence and a chiral interlayer tunneling that creates/annihilates electron-hole pairs in the p-wave channel only. Their competition leads to a rich phase diagram when the heterobilayer band alignment is tuned toward the inverted regime through the interlayer potential difference induced by the gate (i.e., interlayer bias). At a relatively strong dielectric screening, the bias drives transitions from a normal insulator (NI) to three nontrivial phases sequentially: (i) ES, (ii) coexistence of QAH in spin-up and ES in spin-down species (QAH-ES), and (iii) QSH insulator. At weak screening, magnetic order spontaneously develops along with the interlayer coherence, where the heterobilayer can be gate tuned between (iv) a magnetic ES (MES) and (v) a QAH phase. Remarkably, the topologically distinct phases are connected through spontaneous symmetry breaking without gap closing. The gate switchability, together with the sizable QSH/QAH gap that can exceed room temperature, points to practical spintronic highways at the electrically reconfigurable topological interfaces.

RESULTS

Figure 1 schematically explains the gate-controlled phase transitions. TMD heterobilayers have the type II band alignment, where the conduction (valence) band edge consists of upper (lower) massive Dirac cones from the top (bottom) layer, at the K and −K corners of the hexagonal Brillouin zone. Because of the spin-valley locking in TMD monolayers, only the spin-up (down) massive Dirac cones are relevant at the K (−K) valley (*13*). At small or negative E_g (bandgap), a pair of layer-separated electron and hole can be spontaneously generated by their Coulomb interaction or by the interlayer quantum tunneling. For several high-symmetry stacking configurations, the C_3 rotational symmetry dictates the tunneling to have a chiral dependence on the in-plane wave vector ($t \propto k_x \pm ik_y$) (*13*). In the inverted regime ($E_g < 0$), quantum tunneling becomes resonant at $k \sim \sqrt{|E_g|}$, so its effective strength grows with $|E_g|$, the latter becoming a knob to control the dominance between Coulomb interaction and quantum tunneling. Major features of the phase diagram can then be intuitively anticipated.

When an interlayer bias tunes E_g toward the inverted regime, the Coulomb interaction first drives the heterobilayer into ES with spontaneous s-wave interlayer coherence (Fig. 1D), as well studied in TMD double-layer heterostructures designed with interlayer tunneling quenched (*7*, *8*). In contrast to conventional double layers where tunneling will fix the phase of the interlayer coherence (*1*, *2*), here, moderate tunneling of the unique p-wave form does not affect excitons condensed in the s-wave channel. Instead, the chiral tunneling induces a background coherence in the p-wave channel, whose interference with the condensate in the s-wave channel enables in situ measurement on the condensate phase through an in-plane electrical polarization. In this case, the ES phase becomes nematic, with a spontaneous breaking of the rotational symmetry.

Only deep in the inverted regime, the eventual dominance of quantum tunneling pins the interlayer coherence entirely in the p-wave

Department of Physics and Center of Theoretical and Computational Physics, University of Hong Kong, Hong Kong, China.
*Corresponding author. Email: wangyao@hku.hk

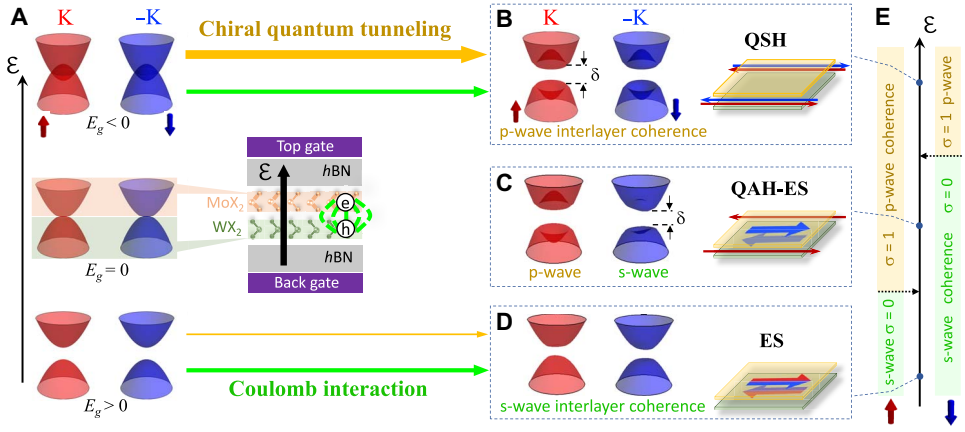

Fig. 1. Band inversion under competition between Coulomb interaction and chiral quantum tunneling. (**A**) Heterobilayers of semiconducting TMDs feature the type II band alignment, where conduction and valence band edges are spin-valley–locked massive Dirac cones from opposite layers. The bandgap E_g in the noninteracting limit can be closed and inverted by an interlayer bias. (**B** to **D**) Phases of the bilayer under the competition between Coulomb and interlayer quantum tunneling of the symmetry dictated chiral form (c.f. text). The dominance of Coulomb at positive small E_g leads to ES of spontaneous s-wave interlayer coherence, shown in (D). The dominance of chiral quantum tunneling at negative E_g pins the interlayer coherence in the p-wave channel, where the bilayer is a QSH insulator, shown in (B). (**E**) Such phase transition occurs nonsimultaneously for spin-up and spin-down species. Between ES and QSH phases, there is a phase of coexistence of ES in spin-down and QAH in spin-up species, as shown in (C).

channel, and the heterobilayer becomes a QSH insulator. Helical edge states appear in the hybridization gap δ (Fig. 1B), the magnitude of which is substantially enhanced by Coulomb interaction compared to the noninteracting case (*13*). The phase transition between ES and QSH does not happen simultaneously for spin-up and spin-down species (Fig. 1E), leaving a bias range for the coexistence of exciton superfluidity in one spin species and QAH in the other. This QAH-ES phase features both counterflow bulk supercurrent and chiral edge state in the bulk gap (Fig. 1C).

In the noninteracting limit, the effect of chiral quantum tunneling in the TMD heterobilayer is well described by the two-band Hamiltonian (*13*): $\hat{H}_{0,\tau} = \sum_{\mathbf{k}} (\hat{a}_{\mathbf{k}}^{\dagger}, \hat{b}_{\mathbf{k}}^{\dagger}) \left[\eta k^2 + \varepsilon_{\mathbf{k}}\sigma_z + t_{\tau\mathbf{k}}\sigma_+ + t_{\tau\mathbf{k}}^{*}\sigma_-\right] (\hat{a}_{\mathbf{k}}, \hat{b}_{\mathbf{k}})^T$, where $\hat{a}_{\mathbf{k}}^{\dagger}$ ($\hat{b}_{\mathbf{k}}$) creates electron (hole) in the top (bottom) layer, $\tau = \pm 1$ is the valley index, σ is the Pauli matrices in layer pseudospin space, and $\varepsilon_{\mathbf{k}} = \hbar^2 k^2/2m + E_g/2$. m is twice the reduced mass of electron and hole, and the ηk^2 term accounts for their mass difference. The interlayer tunneling $t_{\tau\mathbf{k}}$ has a stacking-dependent form. For the example of 2H stacking for epitaxially grown heterobilayers (*19*), we have $t_{\tau\mathbf{k}} = v(\tau k_x - i k_y) t_{vv}^{*}/M$ (*13*), where t_{vv} is the hopping amplitude between the valence band edges of the two layers, v is the Dirac cone Fermi velocity, and M is the bandgap of monolayer TMD. The ground state $|\Psi\rangle = \prod_{\tau\mathbf{k}} (u_{\tau\mathbf{k}} + v_{\tau\mathbf{k}} \hat{a}_{\mathbf{k}}^{\dagger} \hat{b}_{\mathbf{k}}) |0\rangle$ then features a p-wave interlayer coherence: $u_{\tau\mathbf{k}}^{*} v_{\tau\mathbf{k}} \propto -\tau k_x + i k_y$, where the spin Hall conductivity jumps from 0 to 1 at $E_g = 0$.

Coulomb interaction is well accounted for in double-layer geometry by the Hartree-Fock approximation, as adopted in various studies of quantum phases therein (*7*, *20*–*24*). The electron energy is dressed by the interaction with the electron-hole pairs in the ground state $|\Psi\rangle$. The effective interlayer tunneling also gets renormalized by the Coulomb interaction, becoming dependent on the electron-hole coherence in $|\Psi\rangle$. The mean-field interacting Hamiltonian reads $\hat{H}_{\tau} = \Sigma_{\mathbf{k}} (\hat{a}_{\mathbf{k}}^{\dagger}, \hat{b}_{\mathbf{k}}^{\dagger}) \left[\eta k^2 + \xi_{\tau\mathbf{k}}\sigma_z + ((-\Delta_{\tau\mathbf{k}} + t_{\tau\mathbf{k}})\sigma_+ + h.c.)\right] (\hat{a}_{\mathbf{k}}, \hat{b}_{\mathbf{k}})^T$, with $\Delta_{\tau\mathbf{k}} = \Sigma_{\mathbf{k}'} V_{\text{inter}}(\mathbf{k} - \mathbf{k}') u_{\tau\mathbf{k}'}^{*} v_{\tau\mathbf{k}'}$, and $\xi_{\tau\mathbf{k}} \equiv \varepsilon_{\mathbf{k}} - \Sigma_{\mathbf{k}'} V_{\text{intra}}(\mathbf{k} - \mathbf{k}') |v_{\tau\mathbf{k}'}|^2 + e^2 C^{-1} \Sigma_{\tau'\mathbf{k}'} |v_{\tau'\mathbf{k}'}|^2/2$. Here, V_{intra} and V_{inter} are the intralayer and interlayer Coulomb interactions, respectively. The last term in $\xi_{\tau\mathbf{k}}$ is the classical charging energy of the bilayer as a parallel-plate capacitor, with $C \equiv e^2/[2(V_{\text{intra}}(0) - V_{\text{inter}}(0))]$ being the capacitance per unit area. The ground state $|\Psi\rangle$ shall now be solved from the self-consistent gap equation

$$\Delta_{\tau\mathbf{k}} = \sum_{\mathbf{k}'} V_{\text{inter}}(\mathbf{k} - \mathbf{k}') \frac{\Delta_{\tau\mathbf{k}'} - t_{\tau\mathbf{k}'}}{2\sqrt{\xi_{\tau\mathbf{k}'}^2 + |\Delta_{\tau\mathbf{k}'} - t_{\tau\mathbf{k}'}|^2}} \quad (1)$$

This mean-field approach describes well the exciton condensate in TMD double layers with interlayer tunneling quenched (*7*).

Figure 2 shows the phase diagram as a function of dielectric constant and bandgap E_g, calculated from Eq. 1 (see Materials and Methods). Different phases are identified from their distinct interlayer coherence $\Delta_{\tau\mathbf{k}}$ and Hall conductance in the quasiparticle gap. At large and positive E_g, a small electron-hole coherence $\Delta_{\tau\mathbf{k}}$ is induced in the p-wave channel by the quantum tunneling at large detuning (Fig. 2B), where the bilayer is a NI. When E_g is reduced below the exciton-binding energy, there is a sudden switch on of the s-wave interlayer coherence by the Coulomb interaction. The bilayer is still topologically trivial but develops the ES either with or without spontaneous magnetic order (Fig. 2, C or D). Both ES phases have been predicted in TMD double layers with quenched tunneling (*7*), and the inclusion of chiral quantum tunneling here introduces little change on the phase boundaries between them and the NI phase.

We find that the interlayer coherence in the ES ground state is a superposition of s- and p-wave components: $\Delta_{\tau\mathbf{k}} = \tau\Delta_s(\mathbf{k}) e^{-i\tau\theta} - \tau\Delta_p(\mathbf{k}) e^{-i\tau\phi(\mathbf{k})}$, with $\phi(\mathbf{k})$ being the azimuth angle of $\mathbf{k}$, and $\Delta_{s,p}$ are real and positive. The interference leads to a node in $\Delta_{\tau\mathbf{k}}$ at azimuth angle equal to θ (c.f. Fig. 2C). The phase θ of the s-wave component is unrestricted, so spontaneous symmetry breaking due to the Coulomb interaction still occurs. The order parameters corresponding to different θ values are related by the operation $\mathcal{G}(\theta) \equiv e^{-i\tau\theta} \times \mathcal{R}(\theta)$, that is, the gauge transformation plus a spatial rotation by angle θ. This is a U(1) symmetry possessed by both Coulomb interaction and chiral tunneling. Consequently, superfluidity is unaffected even when tunneling is quite strong. Remarkably, such ES features an in-plane electric polarization of azimuth angle $\theta - \tau\pi/2$ (white arrows in Fig. 2, C to E), from the interference between the s- and p-wave

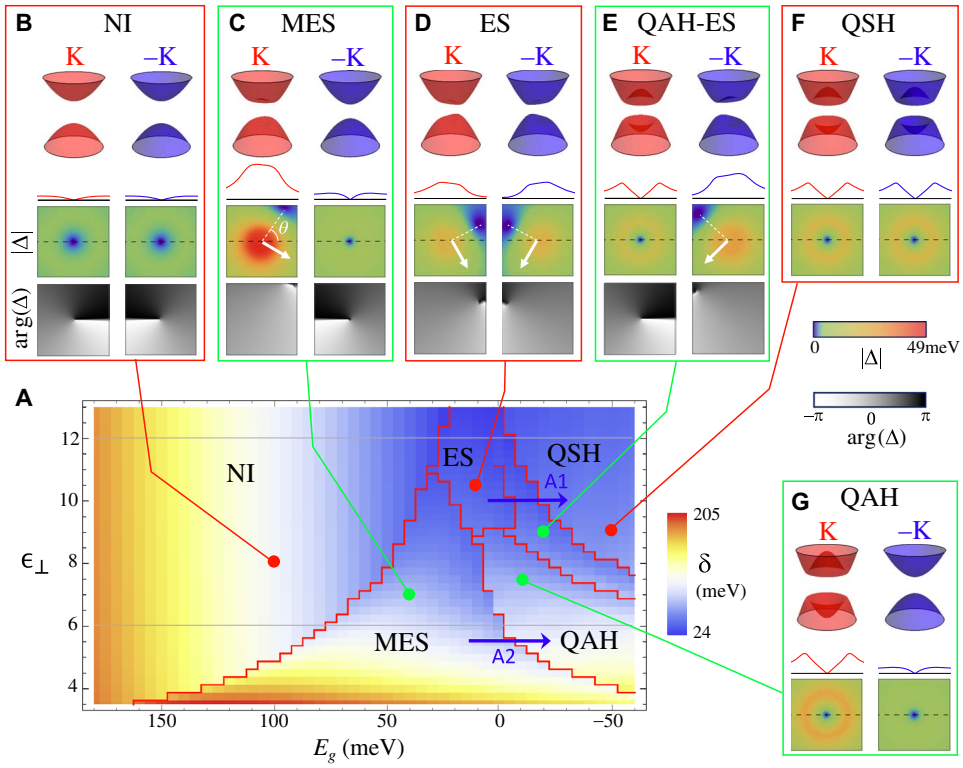

Fig. 2. Phase diagram. (**A**) Phase diagram as a function of bandgap E_g and interlayer dielectric constant $\varepsilon_\perp$. (**B** to **G**) Examples of the six phases. The quasiparticle energy bands are shown, together with the magnitude $|\Delta|$ and phase angle arg(Δ) of the order parameter (see text), over a momentum space region of $[-\pi/8a_0, \pi/8a_0] \times [-\pi/8a_0, \pi/8a_0]$ at the two valleys, respectively, with a_0 being the lattice constant. The curves atop of $|\Delta|$ map show their values along the dashed cut. The QSH and QAH phases have the same p-type arg (Δ) map as in the NI phase. In (C) to (E), the exciton density of the ES is $0.019a_B^{-2}$, $0.028a_B^{-2}$, and $0.029a_B^{-2}$ ($a_B \equiv \hbar^2\varepsilon/me^2$), respectively, and the anisotropic $|\Delta|$ corresponds to an in-plane electric dipole of 6.8*e*Å, 9.0*e*Å, and 8.3*e*Å per exciton, in directions denoted by the white arrows.

components of $\Delta_{\tau\mathbf{k}}$. This makes possible the direct observation of the condensate phase θ.

The spontaneous magnetic order in the exciton condensate arises from a negative exchange interaction between the interlayer excitons (*7*, *25*). The intra- and interlayer Coulomb interactions can be grouped into a repulsive dipole-dipole interaction and an exchange interaction between excitons of the same spin/valley only. The exciton exchange interaction is sensitive to the ratio between the interlayer distance and the exciton Bohr radius and can have a sign change as a function of this ratio (*26*). The Bohr radius is proportional to the dielectric constant ε. At a fixed interlayer distance *d*, the exchange interaction can then change from a repulsive one at large ε that favors an unpolarized condensate to an attractive one at small ε that favors a spin-polarized condensate (*7*, *25*). The boundary between the spin-polarized and unpolarized ES phases is consistent with that found in the TMD double layer of quenched tunneling (*7*). Our calculations show that this boundary can be extrapolated to divide the rest part of the phase diagram at higher excitonic density. At large ε are phases with spin-balanced electron-hole density, and at small ε are spin-polarized phases (Fig. 2).

With E_g decreasing into the inverted regime, there is a general trend for the interlayer coherence to switch from the Coulomb favored s-wave to the tunneling favored p-wave channel, which is a topological phase transition. In the spin-balanced regime, this transition sequentially happens in spin-up and spin-down species (c.f. Fig. 1E), changing the bilayer from the ES to the QAH-ES and

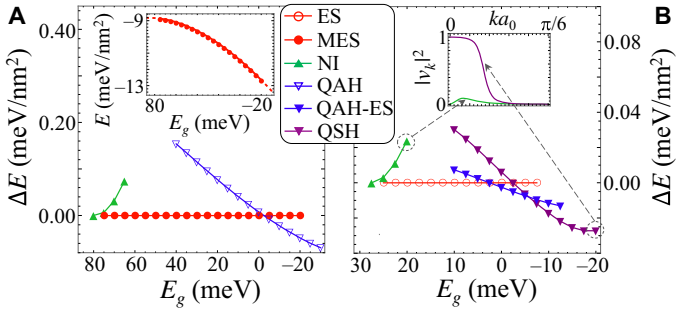

Fig. 3. Topological phase transitions without gap closing. (**A**) Energies of stable solutions of the mean-field Hamiltonian relative to that of the MES state. Inset shows the MES state energy, with the dashed part being the extrapolation. $\varepsilon_\perp = 6$, corresponding to the lower gray horizontal line in Fig. 2A. (**B**) Energies of stable solutions measured from the energy of the ES state. $\varepsilon_\perp = 12$, corresponding to the upper gray horizontal line in Fig. 2A. The NI and topologically nontrivial QSH (QAH) ground states are connected, without gap closing, through the ES (MES) ground state with spontaneous symmetry breaking. Inset of (B) plots the electron-hole pair density $|v_k|^2$ for two representative NI and QSH states.

then to the QSH phase (arrow A1 in Fig. 2A). In the spin-polarized regime, the topological phase transition in the majority spin species changes the bilayer from the MES to QAH (arrow A2 in Fig. 2A). The ES and QAH-ES phase regions both shrink with the increase of ε, showing the right trend toward a direct transition between NI and QSH phases in the infinite ε (noninteracting) limit.

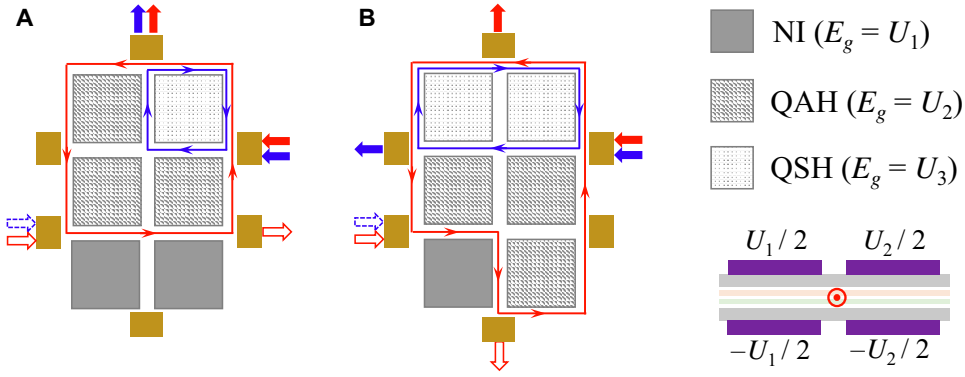

Fig. 4. Configurable spintronics highways. Topological boundaries between NI, QAH, and QSH can be electrically patterned and reconfigured on a bilayer using split top-bottom gate pairs, for wiring protected helical/chiral spin channels. Red and blue colors denote spin-up and spin-down channels, respectively.

DISCUSSION

It is important to point out that a sizable quasiparticle gap remains across all phase regions in Fig. 2A, including the boundaries between topologically distinct phases. This is in contrast to the necessary gap closing in topological phase transitions in the noninteracting limit. Here, the NI phase and the topological nontrivial QSH (QAH) phase are connected through the ES (MES) phase with the spontaneous symmetry breaking. The change of topological number in the ground state is accompanied by the symmetry change, and the gap closing requirement therefore does not apply (*22*, *24*, *27*, *28*). Figure 3 plots the relative energies of the stable solutions of the mean-field Hamiltonian. Both the discontinuity in the first derivative of energy and multiple stable states close to the transition point show that they are first-order quantum phase transitions. Toward the right end of the ES phase regions in Fig. 2A, the electron-hole pair density from our calculations approaches the Mott density (*29*), so likely other correlated phases such as electron-hole plasma can emerge, which is beyond the scope of the mean field approximation here.

The chiral form of the tunneling, ensured here by the threefold rotational symmetry of the heterobilayer lattice, is key to the gate-tunable phases. When the stacking has some deviation from the high-symmetry ones considered, the tunneling can have an s-wave component, which can shrink quantitatively the topological phase regions. Besides, in the presence of s-wave tunneling, as well as the weak trigonal warping effects in TMDs, the interlayer coherence in the ES phase is not completely spontaneous. These two effects can explicitly break the Hamiltonian's U(1) symmetry under $\mathcal{G}(\theta)$. Similar to the role of the interlayer tunneling in conventional double-layer ES (*30*), they will lift the ground-state degeneracy. Consequently, the Goldstone bosons will not be massless but remain relatively light if the trigonal warping and the s-wave tunneling component are not large.

It is also interesting to note that the distinct topological orders of the NI and QSH (QAH) states are reflected in the electron-hole pair density $|v_k|^2$, while their Δ_k plots look the same (Fig. 2). As shown in Fig. 3B, the $|v_k|^2$ plot of the NI state is of the character of the Bose-Einstein condensate (BEC)–type state of tightly bound electron-hole pairs of p-orbital relative motion. In contrast, $|v_k|^2$ of the QSH state is of the character of the Bardeen-Cooper-Schrieffer (BCS) state of weak pairing. This is consistent with earlier work showing that the distinction between BEC and BCS in the p-wave channel is topological (*31*).

The heterobilayers can be formed with a variety of semiconducting TMD compounds that feature similar band structures (*13*), while their different work functions lead to choices on the bandgap. Heterobilayers of MoS_2, $MoSe_2$, WS_2, and WSe_2 have been extensively studied for interlayer excitons in the type II band alignment (*32*). These heterobilayers have a gap of 1 ~ 2 eV, which requires a large electric field to invert. First-principles calculations show that using compounds such as 1H WTe_2, CrS_2, $CrSe_2$, and $CrTe_2$ as one or both building blocks leads to a much smaller gap in the absence of electric field (*13*, *33*, *34*), which can be more favorable choices for device applications, allowing heterobilayers to be tuned in the desired regime by a small electric field.

The gate switchability and the sizable gap that can exceed room temperature in the QSH and QAH phases point to exciting opportunities for practical quantum spintronics by exploring the protected edge states. Using the split top-bottom gate design that has been implemented in bilayer graphene to define valley channels (*35*–*37*), topological boundaries between NI, QAH, and QSH can be programmed on the heterobilayer for wiring the helical/chiral channels to conduct spin currents, as Fig. 4 illustrates. There also lies an intriguing possibility of integrating these topological channels with the counterflow superfluidity when the top and bottom layers are separately contacted.

MATERIALS AND METHODS

In the numerical calculation of the phase diagram and phase transitions presented in Figs. 2 and 3, we adopted the typical forms of the intra- and interlayer Coulomb interactions (*7*): $V_{\text{intra}}(\mathbf{k}) = 2\pi e^2/(\varepsilon k)$ and $V_{\text{inter}}(\mathbf{k}) = V_{\text{intra}}(\mathbf{k})e^{-kd}$. $\varepsilon = \sqrt{\varepsilon_{\parallel}\varepsilon_{\perp}}$, where $\varepsilon_{\parallel}$ ($\varepsilon_{\perp}$) is the intralayer (interlayer) dielectric constant. $d = D\sqrt{\varepsilon_{\parallel}/\varepsilon_{\perp}}$, with D being the geometric interlayer distance. The chiral tunneling $t_{\tau\mathbf{k}} = v(\tau k_x - ik_y)t^*_{vv}/M$. The parameter values $D = 0.62$ nm, $\varepsilon_{\parallel}/\varepsilon_{\perp} = 1.6$, $m = 0.5m_0$ (with m_0 being electron bare mass), $t_{vv} = 14.4$ meV, $v = 3.512$ eV · Å, $M = 1.66$ eV were used here based on first-principles calculations (*13*, *38*–*40*). The valley-coupled gap equation Eq. 1 was numerically solved by convergence to stable solutions with various initial trial $\Delta_{\tau\mathbf{k}}$.

REFERENCES AND NOTES

1. J. P. Eisenstein, A. H. MacDonald, Bose-Einstein condensation of excitons in bilayer electron systems. *Nature* **432**, 691–694 (2004).
2. D. Nandi, A. D. K. Finck, J. P. Eisenstein, L. N. Pfeiffer, K. W. West, Exciton condensation and perfect Coulomb drag. *Nature* **488**, 481–484 (2012).
3. X. Liu, K. Watanabe, T. Taniguchi, B. I. Halperin, P. Kim, Quantum Hall drag of exciton condensate in graphene. *Nat. Phys.* **13**, 746–750 (2017).
4. J. I. A. Li, T. Taniguchi, K. Watanabe, J. Hone, C. R. Dean, Excitonic superfluid phase in double bilayer graphene. *Nat. Phys.* **13**, 751–755 (2017).
5. G. W. Burg, N. Prasad, K. Kim, T. Taniguchi, K. Watanabe, A. H. MacDonald, L. F. Register, E. Tutuc, Strongly enhanced tunneling at total charge neutrality in double-bilayer graphene-WSe_2 heterostructures. *Phys. Rev. Lett.* **120**, 177702 (2018).

6. H. Min, R. Bistritzer, J.-J. Su, A. H. MacDonald, Room-temperature superfluidity in graphene bilayers. *Phys. Rev. B* **78**, 121401(R) (2008).
7. F.-C. Wu, F. Xue, A. H. MacDonald, Theory of two-dimensional spatially indirect equilibrium exciton condensates. *Phys. Rev. B* **92**, 165121 (2015).
8. M. M. Fogler, L. V. Butov, K. S. Novoselov, High-temperature superfluidity with indirect excitons in van der waals heterostructures. *Nat. Commun.* **5**, 4555 (2014).
9. X.-L. Qi, S.-C. Zhang, The quantum spin hall effect and topological insulators. *Phys. Today* **63**, 33–38 (2010).
10. M. Z. Hasan, C. L. Kane, *Colloquium*: Topological insulators. *Rev. Mod. Phys.* **82**, 3045–3067 (2010).
11. X. Qian, J. Liu, L. Fu, J. Li, Quantum spin Hall effect in two-dimensional transition metal dichalcogenides. *Science* **346**, 1344–1347 (2014).
12. Q. Liu, X. Zhang, L. B. Abdalla, A. Fazzio, A. Zunger, Switching a Normal Insulator into a Topological Insulator via Electric Field with Application to Phosphorene. *Nano Lett.* **15**, 1222–1228 (2015).
13. Q. Tong, H. Yu, Q. Zhu, Y. Wang, X. Xu, W. Yao, Topological mosaics in moiré superlattices of van der Waals heterobilayers. *Nat. Phys.* **13**, 356–362 (2017).
14. S. Wu, V. Fatemi, Q. D. Gibson, K. Watanabe, T. Taniguchi, R. J. Cava, P. Jarillo-Herrero, Observation of the quantum spin Hall effect up to 100 kelvin in a monolayer crystal. *Science* **359**, 76–79 (2018).
15. H. Weng, R. Yu, X. Hu, X. Dai, Z. Fang, Quantum anomalous Hall effect and related topological electronic states. *Adv. Physiol. Educ.* **64**, 227–282 (2015).
16. C.-Z. Chang, J. Zhang, X. Feng, J. Shen, Z. Zhang, M. Guo, K. Li, Y. Ou, P. Wei, L.-L. Wang, Z.-Q. Ji, Y. Feng, S. Ji, X. Chen, J. Jia, X. Dai, Z. Fang, S.-C. Zhang, K. He, Y. Wang, L. Lu, X.-C. Ma, Q.-K. Xue, Experimental observation of the quantum anomalous Hall effect in a magnetic topological insulator. *Science* **340**, 167–170 (2013).
17. Z. Fei, T. Palomaki, S. Wu, W. Zhao, X. Cai, B. Sun, P. Nguyen, J. Finney, X. Xu, D. H. Cobden, Edge conduction in monolayer WTe_2. *Nat. Phys.* **13**, 677–682 (2017).
18. S. Tang, C. Zhang, D. Wong, Z. Pedramrazi, H.-Z. Tsai, C. Jia, B. Moritz, M. Claassen, H. Ryu, S. Kahn, J. Jiang, H. Yan, M. Hashimoto, D. Lu, R. G. Moore, C.-C. Hwang, C. Hwang, Z. Hussain, Y. Chen, M. M. Ugeda, Z. Liu, X. Xie, T. P. Devereaux, M. F. Crommie, S.-K. Mo, Z.-X. Shen, Quantum spin Hall state in monolayer 1T′-WTe_2. *Nat. Phys.* **13**, 683–687 (2017).
19. W.-T. Hsu, L.-S. Lu, P.-H. Wu, M.-H. Lee, P.-J. Chen, P.-Y. Wu, Y.-C. Chou, H.-T. Jeng, L.-J. Li, M.-W. Chu, W.-H. Chang, Negative circular polarization emissions from WSe_2/$MoSe_2$ commensurate heterobilayers. *Nat. Commun.* **9**, 1356 (2018).
20. X. Zhu, P. B. Littlewood, M. S. Hybertsen, T. M. Rice, Exciton condensate in semiconductor quantum well structures. *Phys. Rev. Lett.* **74**, 1633–1636 (1995).
21. B. Seradjeh, J. E. Moore, M. Franz, Exciton condensation and charge fractionalization in a topological insulator film. *Phys. Rev. Lett.* **103**, 066402 (2009).
22. D. I. Pikulin, T. Hyart, Interplay of exciton condensation and the quantum spin Hall effect in InAs/GaSb bilayers. *Phys. Rev. Lett.* **112**, 176403 (2014).
23. J. C. Budich, B. Trauzettel, P. Michetti, Time reversal symmetric topological exciton condensate in bilayer HgTe quantum wells. *Phys. Rev. Lett.* **112**, 146405 (2014).
24. F. Xue, A. H. MacDonald, Time-reversal symmetry-breaking nematic insulators near quantum spin Hall phase transitions. *Phys. Rev. Lett.* **120**, 186802 (2018).
25. M. Combescot, R. Combescot, M. Alloing, F. Dubin, Effects of fermion exchange on the polarization of exciton condensates. *Phys. Rev. Lett.* **114**, 090401 (2015).
26. C. Ciuti, V. Savona, C. Piermarocchi, A. Quattropani, P. Schwendimann, Role of the exchange of carriers in elastic exciton-exciton scattering in quantum wells. *Phys. Rev. B* **58**, 7926–7933 (1998).
27. M. Ezawa, Y. Tanaka, N. Nagaosa, Topological phase transition without gap closing. *Sci. Rep.* **3**, 2790 (2013).
28. Y. Yang, H. Li, L. Sheng, R. Shen, D. N. Sheng, D. Y. Xing, Topological phase transitions with and without energy gap closing. *New J. Phys.* **15**, 083042 (2013).
29. R. Maezono, P. L. Ríos, T. Ogawa, R. J. Needs, Excitons and biexcitons in symmetric electron-hole bilayers. *Phys. Rev. Lett.* **110**, 216407 (2013).
30. J.-J. Su, A. H. MacDonald, How to make a bilayer exciton condensate flow. *Nat. Phys.* **4**, 799–802 (2008).
31. N. Read, D. Green, Paired states of fermions in two dimensions with breaking of parity and time-reversal symmetries and the fractional quantum Hall effect. *Phys. Rev. B* **61**, 10267–10297 (2000).
32. P. Rivera, H. Yu, K. L. Seyler, N. P. Wilson, W. Yao, X. Xu, Interlayer valley excitons in heterobilayers of transition metal dichalcogenides. *Nat. Nanotechnol.* **13**, 1004–1015 (2018).
33. F. A. Rasmussen, K. S. Thygesen, Computational 2D materials database: Electronic structure of transition-metal dichalcogenides and oxides. *J. Phys. Chem. C* **119**, 13169–13183 (2015).
34. V. O. Özçelik, J. G. Azadani, C. Yang, S. J. Koester, T. Low, Band alignment of two-dimensional semiconductors for designing heterostructures with momentum space matching. *Phys. Rev. B* **94**, 035125 (2016).
35. I. Martin, Y. M. Blanter, A. F. Morpurgo, Topological confinement in bilayer graphene. *Phys. Rev. Lett.* **100**, 036804 (2008).
36. J. Li, K. Wang, K. J. McFaul, Z. Zern, Y. Ren, K. Watanabe, T. Taniguchi, Z. Qiao, J. Zhu, Gate-controlled topological conducting channels in bilayer graphene. *Nat. Nanotechnol.* **11**, 1060–1065 (2016).
37. Z. Qiao, J. Jung, Q. Niu, A. H. MacDonald, Electronic highways in bilayer graphene. *Nano Lett.* **11**, 3453–3459 (2011).
38. Y. Wang, Z. Wang, W. Yao, G.-B. Liu, H. Yu, Interlayer coupling in commensurate and incommensurate bilayer structures of transition-metal dichalcogenides. *Phys. Rev. B* **95**, 115429 (2017).
39. A. Kumar, P. K. Ahluwalia, Tunable dielectric response of transition metals dichalcogenides MX_2 (M=Mo, W; X=S, Se, Te): Effect of quantum confinement. *Phys. B* **407**, 4627–4634 (2012).
40. D. Xiao, G.-B. Liu, W. Feng, X. Xu, W. Yao, Coupled spin and valley physics in monolayers of MoS_2 and other group-VI dichalcogenides. *Phys. Rev. Lett.* **108**, 196802 (2012).

Acknowledgments: We thank S. Zhang and L.-A. Wu for helpful discussions. **Funding:** This work was supported by the Croucher Foundation (Croucher Innovation Award), the RGC (HKU17302617), and the UGC (AoE/P-04/08) of HKSAR. **Author contributions:** W.Y. conceived and designed the research. Q.Z. performed the calculations and analysis, with input from W.Y., M.W.-Y.T., and Q.T. W.Y. and Q.Z. wrote the manuscript. **Competing interests:** The authors declare that they have no competing interests. **Data and materials availability:** All data needed to evaluate the conclusions in the paper are present in the paper and/or the Supplementary Materials. Additional data related to this paper may be requested from the authors.

Submitted 29 June 2018
Accepted 4 December 2018
Published 18 January 2019
10.1126/sciadv.aau6120

Citation: Q. Zhu, M. W.-Y. Tu, Q. Tong, W. Yao, Gate tuning from exciton superfluid to quantum anomalous Hall in van der Waals heterobilayer. *Sci. Adv.* **5**, eaau6120 (2019).

Gate tuning from exciton superfluid to quantum anomalous Hall in van der Waals heterobilayer

Qizhong Zhu, Matisse Wei-Yuan Tu, Qingjun Tong and Wang Yao

Sci Adv **5** (1), eaau6120.
DOI: 10.1126/sciadv.aau6120